Regular Article

PHYSICAL CHEMISTRY RESEARCH
Published by the
Iranian Chemical Society
www.physchemres.org
info@physchemres.org

Phys. Chem. Res., Vol. 11, No. 4, 747-760, December 2023
DOI: 10.22036/pcr.2022.362088.2195

Physical Study of PVA Filled with Carbon Nanotube and Nano Carbon with Roughness Morphology

A.M. Abdullah[a], L.H. Alwan[a], A.A. Ahmed[b] and R.N. Abed[c,*]

[a]*Department of Chemistry, College of Education, University of Samarra, Salah Al Din, Iraq*
[b]*Polymer Research Unit, College of Science, Al-Mustansiriyah University, Baghdad 10052, Iraq*
[c]*Mechanical Engineering Department, Engineering College, Al-Nahrain University, P. O. Box: 64040, Baghdad, Iraq*
(Received 14 September 2022, Accepted 5 November 2022)

In this work, nanocomposite thin films were prepared from poly(vinyl alcohol) (PVA) mixed with carbon nanotube (CNT) and carbon nanoparticles (CN) using the casted method. Our goal was to produce a PVA texture modified with these nanoparticles. The nanoparticles contents in the nanocomposite thin films were measured by utilizing reflectance and absorbance data. The presence of carbon nanotube and carbon nanoparticle in the modified PVA matrix improved the optical properties such as reflectance, absorption coefficient, refractive index, and extinction factor. The transmittance and reflectance of the nanocomposite thin films (PVA-0.05CNT, PVA-0.05CN, and PVA-0.025CNT-0.025CN) decreased, and the conductivity and dielectric constant increased. The direct led to a decrease in the transition of energy gap from 4.0 eV to 2.9 eV, and the indirect led to a decrease in the transition of energy gap from 4.4 eV to 2.8 eV. Urbach energy increased from 1.238 eV to 2.711 eV after adding these nanoparticles to the PVA texture. The scanning electron microscope was used to evaluate the particle sizes of these nanoparticles after preparation from the experimental method, which used in the PVA lattice to constitute the thin films nanocomposite (PVA-0.05CNT, PVA-0.05CN, and PVA-0.025CNT-0.025CN). The XRD test demonstrated the semi-crystalline structure of the as-prepared nanocomposite thin film. The atomic force microscope (AFM) test was used to exhibit the average roughness and average root mean square. The nanocomposite thin films (PVA-0.025CNT-0.025CN) are used in many applications such as energy devices, fuel cells, display equipment, optoelectronics, and batteries.

Keywords: Poly(vinyl alcohol), Carbon nanotube (CNT), Nano carbon (CN), Optical properties, Average roughness

INTRODUCTION

Poly(vinyl alcohol) PVA is a non-toxic, odorless, thermostable, powdered or granular, and semi-crystalline polymer [1]. It has exceptional ability for charge storage and strong dielectric thin film [2]. Its electrical and optical features can be tailored by doping with nanomaterials. PVA is present in the market with different grades based on hydrolysis degree and viscosity [3,4]. The polymer compound may be improved using a polymer matrix with filler. The filler dimension can be in nanometers or in micrometers to make the polymer nanocomposite; this filler as a nanomaterial affects the physical, chemical, electronic, and optical properties of PVA [5]. Several types of nanomaterials were used for PVA doping such as CuO, NiO, ZnO, SiC, ZnS, Cr_2O_3, CuS, Co_3O_4, CdSe, TiO_2, Cds, SiO_2, and FeO. They were used to fabricate the nanocomposite thin films with improved structural and electrical properties of PVA. Other nanomaterial such as CNT and CN are also used to dope the PVA and produce nanocomposite thin films [6,7].

Therefore, the nanocomposite thin film is the new thin film with modified properties, which cannot be found in the polymer. Polymers such as PVA doesn't have electrical conductivity; modification of PVA by adding the nanomaterials results in a nanocomposite with a good

*Corresponding author. E-mail: rasheed.n.abed@nahrainuniv.edu.iq

structure and a desired conductivity property [8,9]. The nanocomposite has an improved properties due to its combination with nanomaterials such as carbon nanotube (CNT), making it suitable for a wide range of applications [10]. Carbon nanotube (CNT) has many specifications such as thermal properties, electrical conductivity, aspect ratio, and high strength that promote its usage for modification of polymer. It is used to dope a polymer such as PVA to make a new complex that is used in many useful applications such as developing high energy devices, fuel cells, display equipment, and batteries. Thin films with desired dimensions are easily manufactured to be used for mentioned applications [11]. The properties of the PVA can be changed with incorporation of carbon nanotube (CNT) inside it; CNT interacts with the chains of PVA and results in a PVA nanocomposite thin film (PVA-CNT) [12,13]. The nanocomposite thin film such as PVA and multi-wall carbon nanotube (MWCNT) was used to fabricate an electrode (PVC-MWCNT) for electro-sorption of ions from aqueous solutions [14]. The nanocomposite (PVA-MWCNT) was used to alter the conductivity of PVA, improve the dielectric constant in the PVA matrix, and study the transportation of electrons in thin films when subjected to alternate current (AC) and (DC) direct current [15]. The other nanomaterial used in this work is nano carbon (CN); it is used to dope the PVA and make a nanocomposite thin film (PVA-CN). The goal is to use carbon nanotube (CNT) and nano carbon (CN) in the PVA lattice to improve the PVA's electrical conductivity and make new nanocomposites for using in many applications. Poly(vinyl alcohol) and polyethylene glycol (PEG) thin films correlated with surface engineered multiwalled carbon nanotubes (SE-MWCNTs) have been synthesized to inspect the gases permeated through these thin films, such as CO_2, methane (NH_4), and nitrogen (N_2).Carbon nanotubes possess a microporous structure used in gas separation; they are composed of a hexagonal carbon ring-shaped as the honeycomb. Then, the synthesized thin films possess new structures after adding the carbon nanotubes [16].

In the present work, PVA has been modified by CNT and CN. Characterization of optical properties of the blank PVA and PVA thin films composites (PVA-CNT and PVA-CN) were done; data analysis was done to calculate the optical properties and urbach energy. Also, the XRD test demonstrated the semi-crystalline structure of the nanocomposite thin films of PVA. The aim of this work is to produce a new nanocomposite thin film that possesses good conductivity during the light exposure.

The surface roughness of the thin films was characterized by an atomic force microscope. These thin films are used in many applications such as energy devices, fuel cells, display equipment, optoelectronics, and batteries.

EXPERIMENTAL

Materials

The pure PVA material was purchased from local market in Iraq. The carbon nanotube (CNT) and carbon nano (CN) were synthesized in the lab.

Synthesis Carbon Nanotube and Nano Carbon

The carbon nanotube (CNT) and nano carbon (CN) were synthesized in the lab. Firstly, extraction of carbon nanotube (CNT) was done by picking 1 g of reeds with 3 g of NaOH (1:3 wt.%); the two materials were blended and put down in the furnace at 1 h until the temperature reached 550°C. Then, the temperature raised 10 °C each 1 min, while the calcination was happened after burning at 550 °C. The output was cooled at room temperature and rinsed many times with hot water. Neutralization was done by using hydrochloric acid (HCL) to reach a pH of 7 and get rid of NaOH. Then, the moist mass was quitted and dried for 12 h at 80 °C. Secondly, a same method was utilized to make nano carbon (CN), with the difference in burning the reeds with NaOH for 3 h at 700 °C in the furnace. A Scheme 1 described a flow chart of the main steps for preparing the carbon nanotubes and the nano carbon.

Preparation Thin Film

Initially, 1g of PVA was dissolved in 25 ml of distilled water using continuous stirring at 60 °C for more than 8 h. The gained solution was cooled to a room temperature for about 4 h. Then, some of this mixture was poured in a glass template to make the blank PVA. The rest of solution was blended with 0.05 g of carbon nanotube (CNT) and added to 10 ml distilled water. They were immersed on a beaker for 20 min to gain a suspension solution and by using ultrasonic to mix the solution with CNT homogeneously. The solution

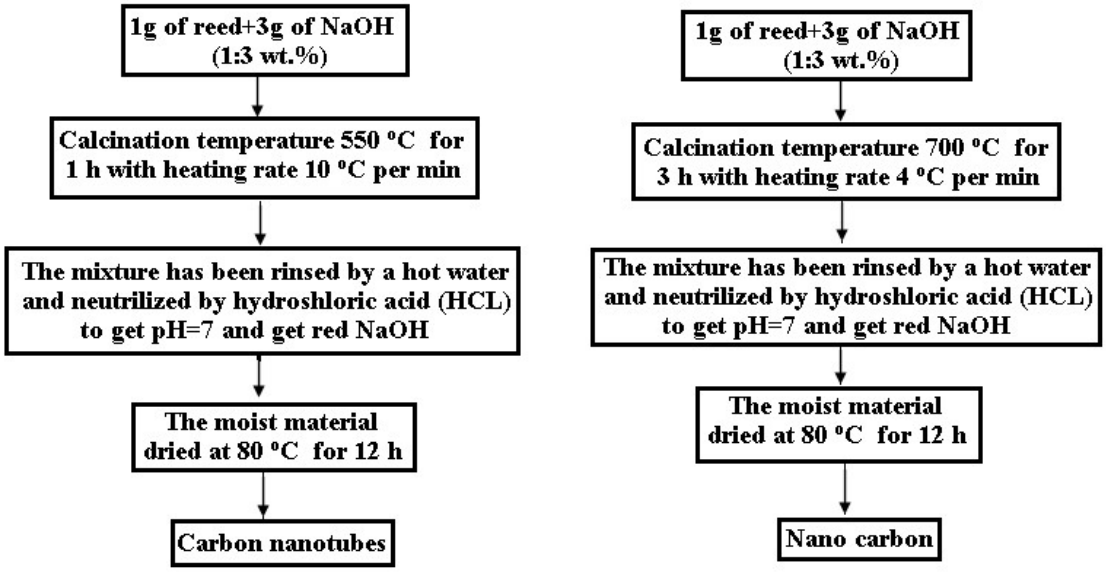

Scheme 1. A flow chart of the main steps for preparing carbon nanotubes and nanocarbon

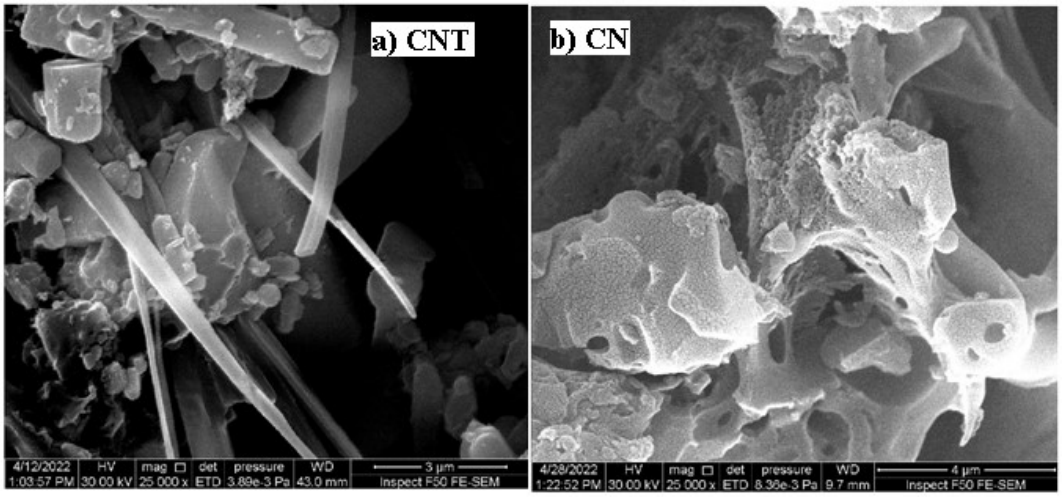

Fig. 1. The images of: a) carbon nanotube (CNT) and b) nano carbon (CN).

of CNT suspension was added dropwise to PVA solution with stirring repeatedly; The PVA-CNT nanocomposite was prepared by this procedure. Finally, PVA-CNT nanocomposite thin film was casted in glass template and left in an oven at 60 °C to dry for about 72 h. The nanocomposite thin film PVA-CN was made from PVA and nano carbon (CN) by the same mentioned method.

Examination Techniques

The Avantes (DH-S-BAL-2048, UV-Vis Spectro-2048) in the wavelength range (250-1300 nm) was used to study the samples by the reflectance for 0.5 step wavelength. The AFM (AA2000) was employed to study the roughness and particles size of the blank PVA and PVA-CNT, PVA-CN, PVA-CNT-CN nanocomposite thin films.

The S50 scanning electron microscopy (SEM) 3 nm at 30 kV SE (low vacuum) was used to illustration the shape after burned. The carbon nanotube after calcination at 550 °C is shown in Fig. 1a and the nano carbon after calcination at 700 °C is shown in Fig. 1b.

The XRD diffraction has the specification as Cu K-alpha 1.54056 Å with very high clarify. The patterns were inspected under 2θ between angles (10°-80°) at 40 kV and 250 mA. The structure properties of the blank PVA and the nanocomposite thin films (PVA-0.05CNT, PVA-0.05CN, and PVA-0.025CNT-0.025CN), shown in Fig. 2, were studied by the XRD diffraction equipment, where it exhibited a semi crystalline structure for the nanocomposite thin film [17].

The nature of the structure is semi crystalline and exhibits one peak for all nanocomposite thin film except the blank PVA; this peak has a broad base confined between 15° to 20° degrees. The XRD test proved that the PVA was doped by CNT and CN. A semi crystalline structure for all nanocomposite thin film was shown [17].

RESULTS AND DISCUSSION

Reflectance for the Blank PVA and Thin Films (PVA-CNT, PVA-CN, and PVA-CNT-CN)

Figure 3 shows the reflectance of the blank PVA and that of nanocomposite thin films (PVA-0.05CNT, PVA-0.05CN, and PVA-0.025CNT-0.025CN).

From Fig. 3, the blank thin film had a high reflectance, but the other doped thin films had very low values of the reflectance in the visible region. The doped thin films (PVA-0.05CNT and PVA-0.05CN) had a reflectance value in the visible region (400-800 nm) that was < 3.0%; the reflectance raised slightly to a value < 4.5% with an increase in the wavelength. The other thin film (PVA-0.025CNT-0.025CN) had a reflectance < 3.0% in the visible region was constant at this value along the axis of the wavelength [18-20].

The Absorbance Coefficient for the Blank PVA and Thin Films (PVA-CNT, PVA-CN, and PVA-CNT-CN)

The absorption coefficients (α) for the blank PVA and the nanocomposite thin films (PVA-0.05CNT, PVA-0.05CN, and PVA-0.025CNT-0.025CN) are shown in Fig. 4.

The value for the blank PVA and the nanocomposite thin films (PVA-0.05CNT, PVA-0.05CN, and PVA-0.025CNT-0.025CN) was calculated using Eq. (1) [21-23]:

$$\alpha = 2.303 * \frac{A}{t} \quad (1)$$

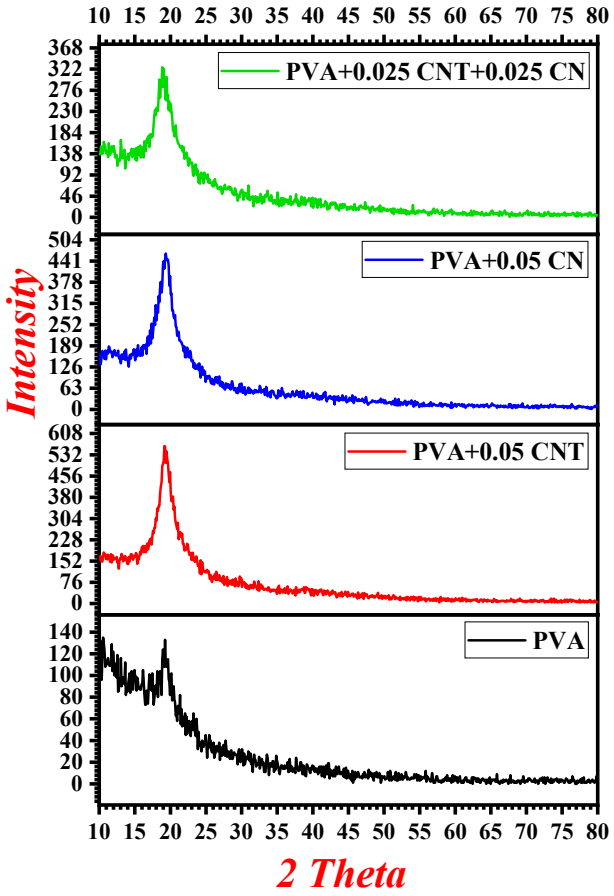

Fig. 2. XRD test for the blank PVA and nanocomposite thin films (PVA-0.05CNT, PVA-0.05CN, and PVA-0.025CNT-0.025CN).

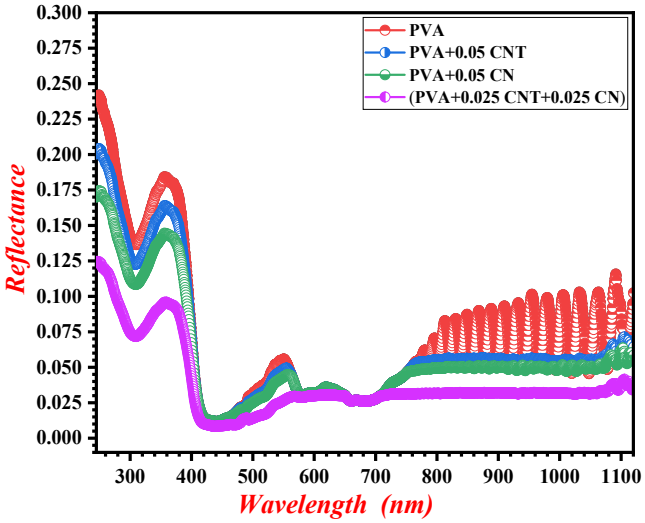

Fig. 3. The reflectance distinction with wavelength for the blank PVA and nanocomposite thin films (PVA-0.05CNT, PVA-0.05CN, and PVA-0.025CNT-0.025CN).

Here, α is the absorbance coefficient (cm^{-1}), A is the absorbance value, and t is the coating thickness (cm).

It is clear from Fig. 4 that the absorption coefficient (α) of the blank PVA didn't have a stable value with the wavelength; it was fluctuating along the wavelength axis. But, the thin films (PVA-0.05CNT, PVA-0.05CN, and PVA-0.025CNT-0.025CN) had absorption coefficient (α) in the same trend through the UV-Vis-IR regions with the wavelength. Therefore, in Fig. 4, there are small humps in the curves of the nanocomposite thin films (PVA-0.05CNT, PVA-0.05CN, and PVA-0.025CNT-0.025CN) that are related to formation of the charges in transport complexes of the particles [24,25].

The Transmittance for the Blank PVA and Thin Films (PVA-CNT, PVA-CN, and PVA-CNT-CN)

The transmittance of blank PVA and nanocomposite thin films (PVA-0.05CNT, PVA-0.05CN, and PVA-0.025CNT-0.025CN) are shown in Fig. 5.

As shown in Fig. 5, the transmittance is 100% in the UV region and a part of the visible region. The blank PVA had a higher transmittance than the other thin films and showed fluctuation (up and under) when the wavelength increased. When the wavelength λ > 560 nm, the transmittance was lower and reached <55% after adding the (CNT and CN) to the nanocomposite thin films of PVA. After adding the nanoparticles CNT and CN, the inner side of the PVA texture might act as scattering stations, which caused a decrease in transmittance. In the curves, the rise and decline are due to the aggregation of nanoparticles inside the PVA texture, causing these shapes for the nanocomposite [25,26].

The Refractive Index for the Blank PVA and Thin Films (PVA-CNT, PVA-CN, and PVA-CNT-CN)

The difference between the curves depends on the distribution of the nanoparticles in the texture of PVA. The refractive index exhibits the propagation for the wavelength inside the thin films (PVA-0.05CNT, PVA-0.05CN, and PVA-0.025CNT-0.025CN). The refractive index is calculated by using the Eq. (2) [27]:

$$n = \left[\frac{1+R}{1-R}\right] + \sqrt{\frac{4R}{(1-R)^2} - k^2} \quad (2)$$

Here, n is refractive index, R is reflectance, and k is extinction factor.

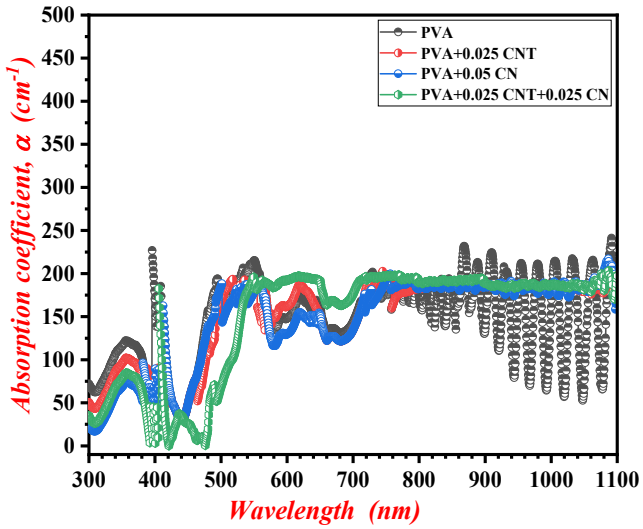

Fig. 4. The absorbance coefficient with wavelength distinction for the blank PVA and nanocomposite thin films (PVA-0.05CNT, PVA-0.05CN, and PVA-0.025CNT-0.025CN).

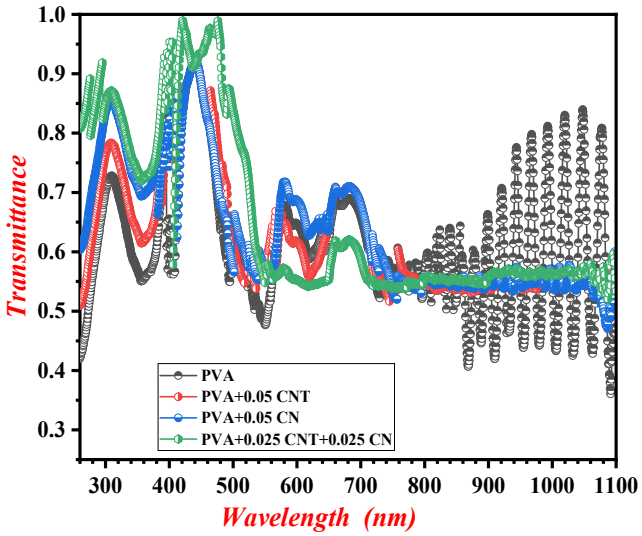

Fig. 5. The transmittance distinction with wavelength for the blank PVA and nanocomposite thin films (PVA-0.05CNT, PVA-0.05CN, and PVA-0.025CNT-0.025CN).

The curves of blank PVA and the nanocomposite thin films (PVA-0.05CNT, PVA-0.05CN, and PVA-0.025CNT-0.025CN) are shown in Fig. 6.

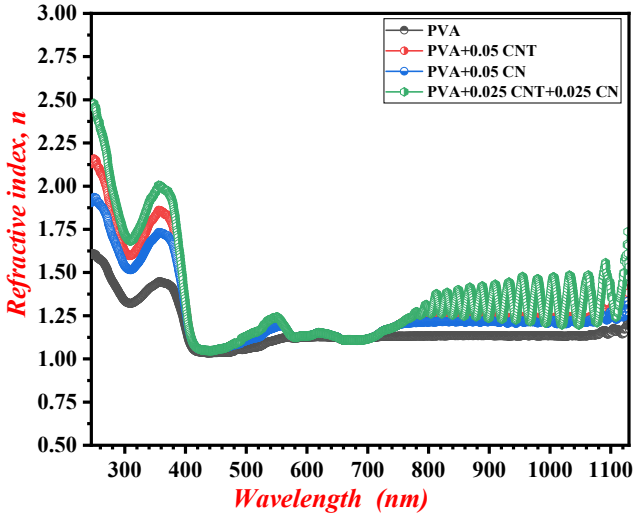

Fig. 6. The refractive index with wavelength distinction for the blank PVA and nanocomposite thin films (PVA-0.05CNT, PVA-0.05CN, and PVA-0.025CNT-0.025CN).

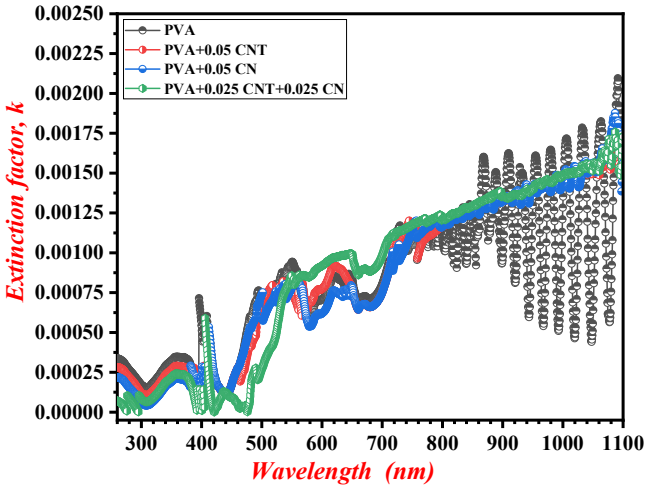

Fig. 7. The extinction factor with wavelength distinction for the blank PVA and nanocomposite thin films (PVA-0.05CNT, PVA-0.05CN, and PVA-0.025CNT-0.025CN).

In Fig. 6, the refractive index for the blank PVA has a low value, but for the nanocomposite thin films (PVA-0.05CNT, PVA-0.05CN, and PVA-0.025CNT-0.025CN), the indexes are increased after incorporation of carbon nanotube (CNT) and nano carbon (CN) in the PVA texture. The increase in the refractive index is dependent on the distribution of CNT and CN in the internal structure of PVA and the filling density of them. The filling density leads to a decrease in the absorption loss inside the nanocomposite thin films of PVA [28,29].

The Extinction Factor for the Blank PVA and Thin Films (PVA-CNT, PVA-CN, and PVA-CNT-CN)

The difference between the curves of absorptions depends on the scattering of the nanoparticles in the PVA texture. The extinction factor exhibits the absorption losses inside the thin films. Figure 7 shows the curves of the blank PVA and the nanocomposite thin films (PVA-0.05CNT, PVA-0.05CN, and PVA-0.025CNT-0.025CN).

The extinction factor is calculated using Eq. (3) [27]:

$$k = \frac{\alpha\lambda}{4\pi} \quad (3)$$

Here, λ is wavelength (cm) and α is absorption coefficient (cm^{-1}).

From Fig. 7, the extinction factor increased with an increase in the wavelength after adding the carbon nanotube (CNT) and the nano carbon (CN) into the PVA lattice. The increase in extinction factor is attributed to an increase in the absorption of the incident light through the thin films (PVA-0.05CNT, PVA-0.05CN, and PVA-0.025CNT-0.025CN). The existence of nanoparticles such as CNT and CN leads to a decrease in the loss of absorbance. Therefore, from figure 7, it can be seen that all the values of the extinction factor are very low for the nanocomposite thin films (PVA-0.05CNT, PVA-0.05CN, and PVA-0.025CNT-0.025CN) and there is a high absorption [30].

The Dielectric Constant for the Blank PVA and Thin Films (PVA-CNT, PVA-CN, and PVA-CNT-CN)

The conduction in PVA as a polymer is very important in the present study. Dielectric constant for the nanocomposite thin films (PVA-0.05CNT, PVA-0.05CN, and PVA-0.025CNT-0.025CN) was calculated. The real and imaginary dielectric constant was calculated by using Eq. (4) [23]:

$$[(\varepsilon) = \varepsilon'(\omega) + i\varepsilon''(\omega)] \quad (4)$$

The dielectric constant (ε) in terms of n and k was calculated using Eq. (5) [23]:

$$\begin{bmatrix} \varepsilon' = n^2 - k^2 \\ \varepsilon'' = 2nk \end{bmatrix} \quad (5)$$

Moreover, both the real $\varepsilon'$and imaginary ε'' for the blank PVA and the nanocomposite thin films (PVA-0.05CNT, PVA-0.05CN, and PVA-0.025CNT-0.025CN) are demonstrated in Figs. 8 and 9.

Figure 8 exhibits the variation of real dielectric constant for the blank PVA and nanocomposite thin films (PVA-0.05CNT, PVA-0.05CN, and PVA-0.025CNT-0.025CN). It is clear from Fig. 8 that the real dielectric constant for the blank PVA has a value of $\varepsilon' = 1.25$. For the nanocomposite thin films (PVA-0.05CNT, PVA-0.05CN, and PVA-0.025CNT-0.025CN), it has a value of $\varepsilon' = 1.75$. An increase in real dielectric constant (ε') is attributed to the addition of the carbon nanotube (CNT) and the nano carbon (CN) to the PVA texture. An increase in ε' leads to an increase in absorption, leading to an increase in the polarization effect of the thin films [25].

Figure 9 exhibits the variation of imaginary dielectric constant for the blank PVA and nanocomposite thin films (PVA-0.05CNT, PVA-0.05CN, and PVA-0.025CNT-0.025CN) with the wavelength.

Also, it was observed from Fig. 9 that the imaginary dielectric constant for the blank PVA fluctuated with an increase in the wavelength; it increases for the nanocomposite thin films (PVA-0.05CNT, PVA-0.05CN, and PVA-0.025CNT-0.025CN). This increase depends on addition of the carbon nanotube (CNT) and the nano carbon (CN) to the PVA texture. The imaginary part provides the dissipative power of the wavelength through the thin layer of the thin films. It demonstrates that when the imaginary part has a low value, the absorption for these thin films is high. It is clear from Fig. 9 that the values of the imaginary part are very low, leading to low value for the dissipative power [31].

The Optical Conductivity for the Blank PVA and Thin Films (PVA-CNT, PVA-CN, and PVA-CNT-CN)

The electrical conductivity that results from the movement of the charge carriers owing to the discontinuous electric field of the incident waves is called optical conductivity, and it is calculated using the Eq. (6) [32]:

$$\sigma = \frac{\alpha n c}{4\pi} \quad (6)$$

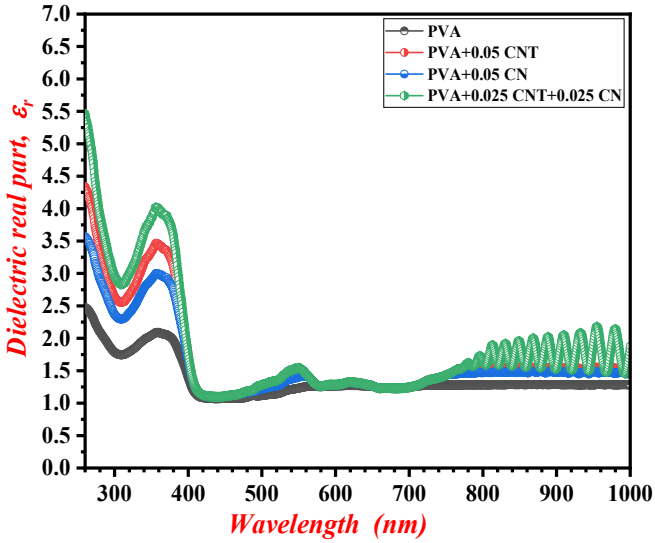

Fig. 8. The real dielectric constant with wavelength distinction for the blank PVA and nanocomposite thin films (PVA-0.05CNT, PVA-0.05CN, and PVA-0.025CNT-0.025CN).

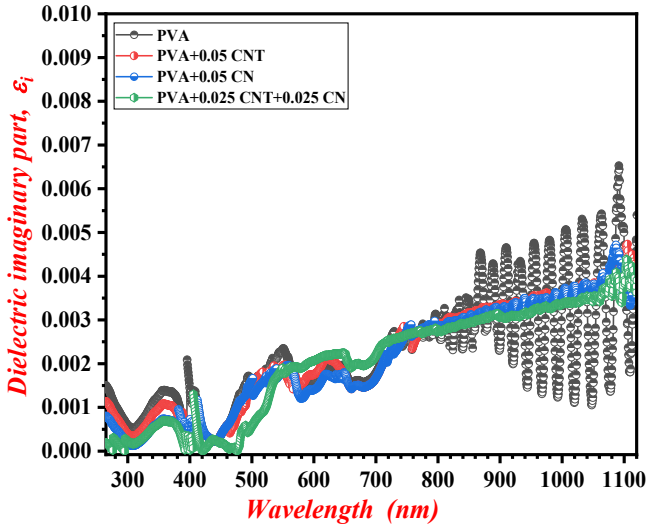

Fig. 9. The imaginary dielectric constant with wavelength distinction for the blank PVA and nanocomposite thin films (PVA-0.05CNT, PVA-0.05CN, and PVA-0.025CNT-0.025CN).

Here, σ is optical conductivity (S^{-1}), c is light speed (3×10^{10} cm s^{-1}), n is refractive index, and α is absorbance coefficient (cm^{-1}).

Figure 10 exhibits the optical conductivity for the blank PVA and the nanocomposite thin films (PVA-0.05CNT, PVA-0.05CN, and PVA-0.025CNT-0.025CN).

From Fig. 10, the optical conductivity varies with the wavelength, where it increases with an increase in the wavelength for the nanocomposite thin films (PVA-0.05CNT, PVA-0.05CN, and PVA-0.025CNT-0.025CN), and due to the electron excitation in the orbit by the wavelength. Therefore, adding the carbon nanotube (CNT) and the nano carbon (CN) to the PVA lattice led to an increase in the charge carriers and an increase in the localized states inside the gap [33,34].

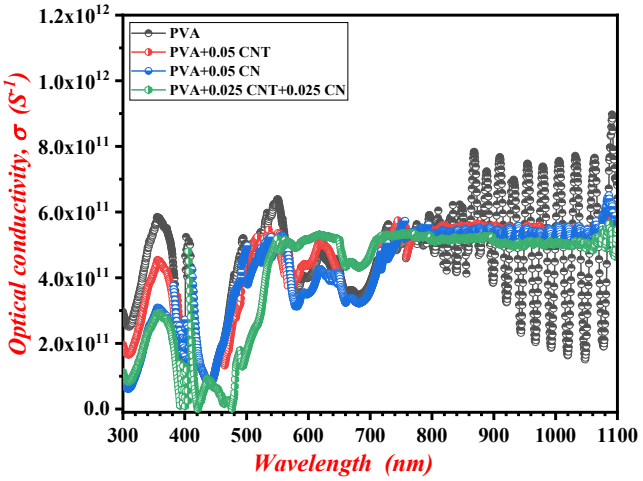

Fig. 10. The optical conductivity with wavelength distinction for the blank PVA and nanocomposite thin films (PVA-0.05CNT, PVA-0.05CN, and PVA-0.025CNT-0.025CN).

The Energy Gap for the Blank PVA and Thin Films (PVA-CNT, PVA-CN, and PVA-CNT-CN)

The absorption coefficient with photon energy was studied to calculate the energy gap for the blank PVA and nanocomposite thin films (PVA-0.05CNT, PVA-0.05CN, and PVA-0.025CNT-0.025CN) for the inter band transmission. The energy gap was calculated using Eq. (7) [35]:

$$\alpha h\nu = B\,(h\nu - E_g)^n \qquad (7)$$

Here, *B* is constant, *Eg* is energy gap, and n is power to the transition type (n = 2 for indirect transition and n = 1/2 for direct transition) [35,36].

The calculated direct energy gap and indirect energy gap from the fitting of $(\alpha h\nu)^2$ against the photon energy for the blank PVA and nanocomposite thin films (PVA-0.05CNT, PVA-0.05CN, and PVA-0.025CNT-0.025CN) are shown in Figs. 11 and 12. The extrapolation intercept for the linear part of the photon energy with zero absorbance and the energy gap value was taken for these thin films [37].

The direct energy gap for the blank PVA and nanocomposite thin films (PVA-0.05CNT, PVA-0.05CN, and PVA-0.025CNT-0.025CN) was shown in Fig. 11. It is clear from Fig. 11 that the value of the energy gap of blank PVA was 4.0 eV that changed to 3.95 after inserting the carbon nanotube (CNT) in the PVA texture. In addition, after inserting the nano carbon, two values of energy gap (2.9 eV and 4.05 eV) were obtained. After inserting the two types of nanoparticles (CNT and CN) into the PVA texture, the energy gap was 2.95 eV. These results shows that by

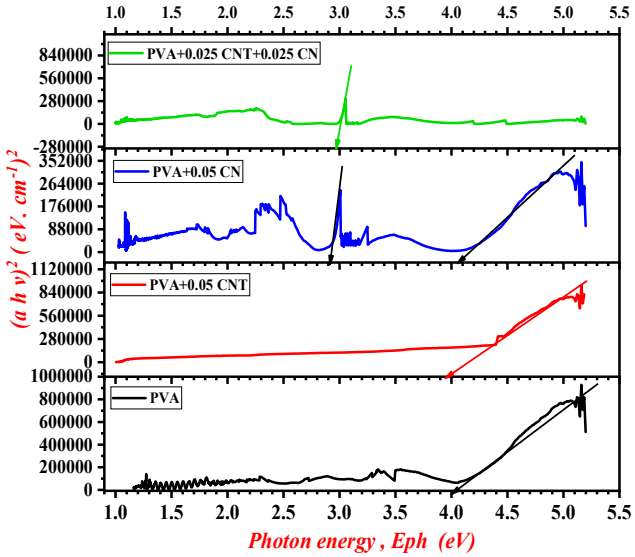

Fig. 11. Variation of $(\alpha h\nu)^2$ with the photon energy ($h\nu$) for the semi-crystalline nanocomposite thin films of the blank PVA and (PVA-0.05CNT, PVA-0.05CN, and PVA-0.025CNT-0.025CN).

inserting the CNT and CN to the PVA texture, the energy gap for the nanocomposite thin films of PVA decreases; the mentioned values are shown in a Table 1 [38,39,40].

In comparison with Fig. 11, Fig. 12 shows the relation between $(\alpha h\nu)^{0.5}$ and photon energy ($h\nu$).

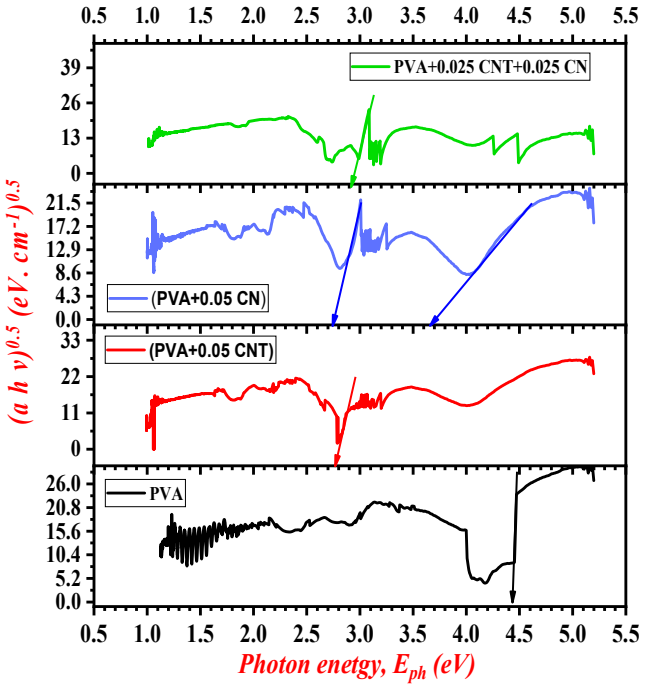

Fig. 12. Variation of $(\alpha hv)^{0.5}$ with the photon energy (hv) for the semi-crystalline nanocomposite thin films of the blank PVA and (PVA-0.05CNT, PVA-0.05CN, and PVA-0.025CNT-0.025CN).

From Fig.12, the value of the indirect energy gap for the blank PVA was 4.4 eV. After inserting the CNT in the PVA texture, the energy gap was 2.8 eV, and after insertion of CN in the PVA texture, the energy gap had two values of 2.75 eV and 3.65 eV. However, by inserting the CNT and CN inside the PVA texture, the energy gap decreased to 2.9 eV. Therefore, by inserting the CNT and CN in the PVA texture, there is a decrease in the energy gap for the nanocomposite thin films of PVA; the mentioned values are shown in a Table 1 [31,41,42].

The decrease in direct and indirect energy gap is due to the powerful interaction between the electrons conducts, and the magnetic moment in the atom decreases the localized states between bands, leading to a change in the energy gap of PVA as a host for the nanoparticles [43].

The Urbach Energy for the Blank PVA and Thin Films (PVA-CNT, PVA-CN, and PVA-CNT-CN)

The electron transmission for the nanocomposite thin films is understood from the local states between bands, indicating the level of defects that exist between the bands. Urbach energy is calculated using Eq. (8) [37,44]:

$$\alpha = \alpha_o \exp \frac{h\nu}{E_u} \quad (8)$$

The revised version of Eq. (8) results in Eq. (9):

$$\ln\alpha = \ln\alpha_o + \frac{h\nu}{E_u} \quad (9)$$

Here, α_o is constant.

The urbach energy is shown in Fig. 13; it is found from the variation of natural logarithm of absorbance coefficient with photon energy.

To calculate the urbach energy (Fig. 13), the inverse slope of the straight line for all curves was evaluated. Figure 13 exhibits the values of urbach energy for the nanocomposite thin films (PVA-0.05CNT, PVA-0.05CN, and PVA-0.025CNT-0.025CN); the urbach energy increased from 2.205 eV to 2.711 eV after adding the carbon nanotube (CNT) and nano carbon (CN), leading to an increase in the localized states in the band gap. The values of urbach energy are shown in Table 1 [45,46].

Table 1. The Values of Direct Energy Gap, Indirect Energy Gap, and Urbach Energy

No.	Parameters	Blank PVA	PVA+0.05CNT	PVA+0.05CN	PVA+0.025CNT +0.025CN
1	Direct transition of (Eg) (eV)	4.0	3.95	2.90, 4.05	2.95
2	Indirect transition of (Eg) (eV)	4.40	2.8	2.75, 3.65	2.9
3	Urbach energy (Eu) (eV)	1.238	2.515	2.205	2.711
4	(α_o) constant (cm^{-1})	223.11	427.28	288.25	488.73

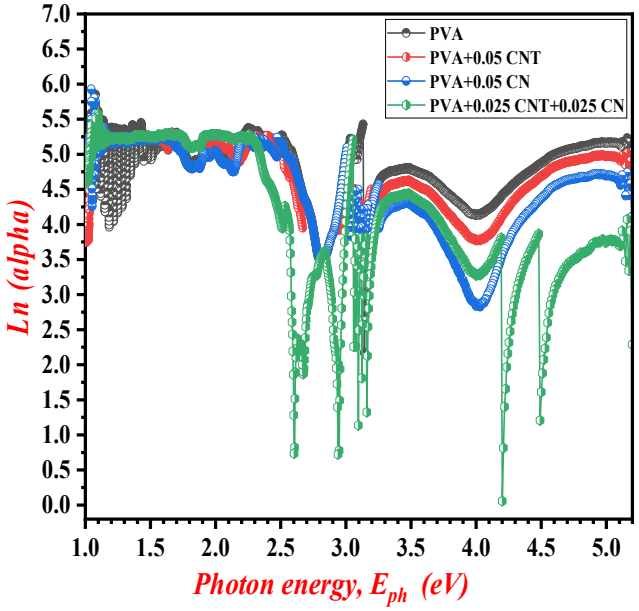

Fig. 13. The urbach energy with photon energy distinction for the blank PVA and nanocomposite thin films (PVA-0.05CNT, PVA-0.05CN, and PVA-0.025CNT-0.025CN).

THE AFM PICTURES FOR THE BLANK PVA AND THIN FILMS (PVA-CNT, PVA-CN, AND PVA-CNT-CN)

The AFM images for the blank PVA and the nanocomposite thin films (PVA-0.05CNT, PVA-0.05CN, and PVA-0.025CNT-0.025CN) are shown in Figs. 14a, 14b, 14c and 14d). It shows the distribution of carbon nanotube (CNT) and nano carbon (CN) in the PVA texture, showing the roughness and average root mean square. The AFM images showed brown areas that specify valleys, and the brightened regions that display the peak point of the nanocomposite surface. According to the AFM images, the surface of the blank PVA had average roughness of 0.547 nm, and the root mean square was 0.901 nm (Fig. 14a). The surface of the carbon nanotube (CNT) with PVA had an average roughness of 0.979 nm, and the root means square was 1.52 nm, shown in Fig. 14b. Also, the surface of nano carbon (CN) with PVA had an average roughness of.17 nm, and the root mean square was 1.79 nm, shown in Fig. 14c. Finally, the surface of CNT and CN with PVA had an average roughness of 4.86 nm, and the root means square was 6.18 nm, shown in Fig. 14d. The values of roughness and root mean square are shown in Table 2 [47,48].

CONCLUSIONS

The poly(vinyl alcohol) (PVA) was mixed with carbon nanotube (CNT) and carbon nanoparticles (CN) to make thin films using the casted method. The concentration of CNT and CN particles affected the PVA texture properties. The optical properties such as reflectance, absorption coefficient, refractive index, and extinction factor were calculated for the PVA modified with CNT and CN. The transmittance and reflectance of the nanocomposite thin films (PVA-0.05CNT, PVA-0.05CN, and PVA-0.025CNT-0.025CN) decreased, but the conductivity and dielectric constant increased. The direct led to a decrease in transition of energy gap from 4.0 eV to 2.9 eV, compared to the energy gap of blank PVA that was 4.0 eV. The indirect led to a decrease in transition of energy gap from 4.4 eV to 2.8 eV, compared to the energy gap of blank PVA that was 4.4 eV. Urbach energy increased from 1.238 eV to 2.711 eV after adding the CNT and CN to the PVA texture, due to an increase in the localized states of the gap. The form of CNT and CN were tested by SEM to evaluate their structures. The XRD test proved that the structure of the PVA nanocomposite thin film was semi-crystalline. The surface morphology of the nanocomposite thin films (PVA-0.05CNT, PVA-0.05CN, and PVA-0.025CNT-0.025CN) was tested by AFM. It showed that after adding the CNT and CN, the average roughness increased from 0.547 nm (for the blank PVC) to 4.86 nm and the average root mean square increased from 0.901 nm to 6.81. Increase in the roughness led to an increase in the absorbance. The nanocomposite thin films (PVA-0.05CNT, PVA-0.05CN, and PVA-0.025CNT-0.025CN) are used in many applications such as energy devices, fuel cells, display equipment, optoelectronics, and batteries.

ACKNOWLEDGMENTS

This work was supported by Polymer Research Center/ College of Science of Al-Mustansiriyah University.

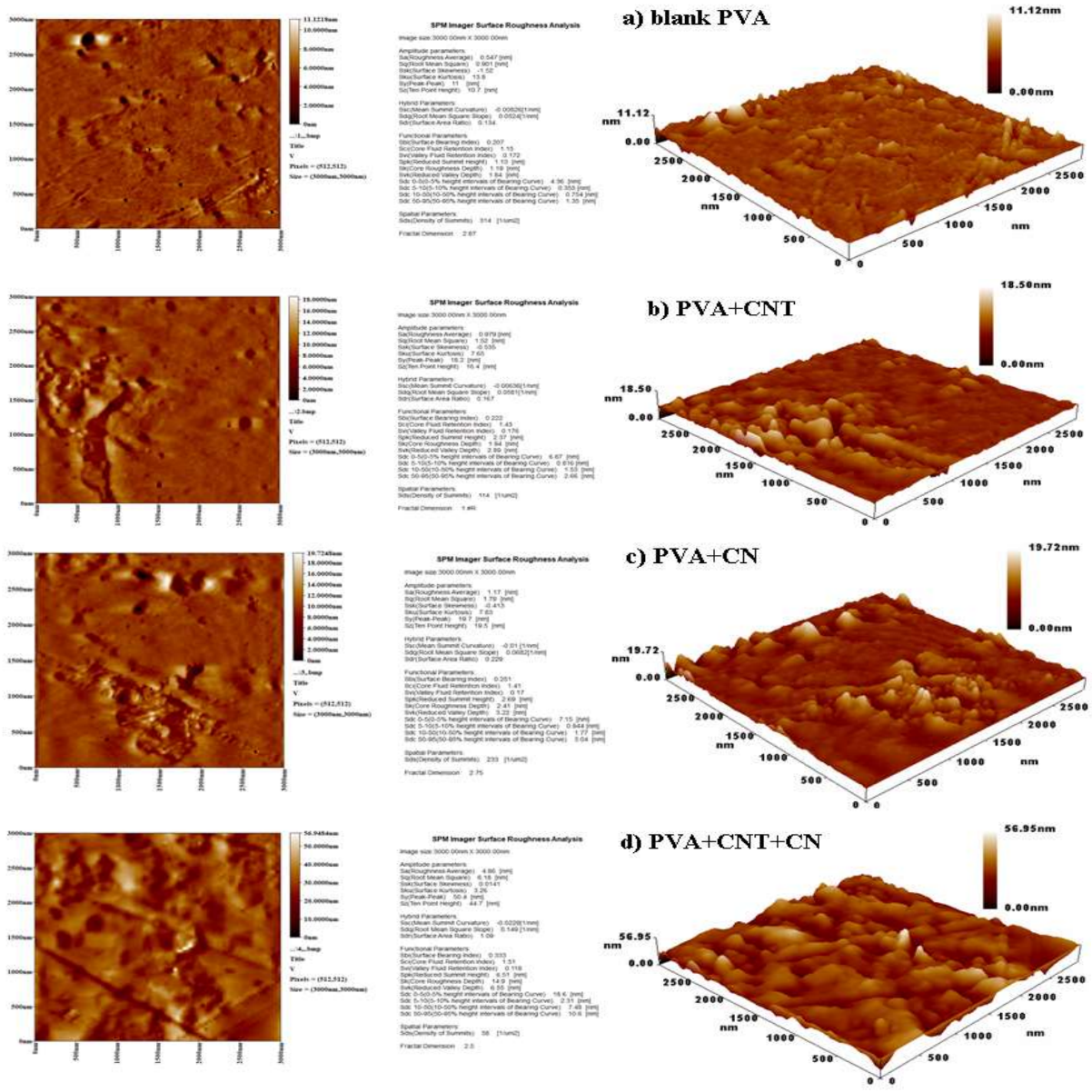

Fig. 14. 3D and 2D images display the average roughness and root mean square for: a) blank PVA, b) PVA-0.05 CNT, c) PVA-0.05 CN, and d) PVA-0.025 CNT-0.025 CN.

Table 2. The AFM Images for the Blank PVA and the Nanocomposites Thin Films (PVA-0.05CNT, PVA-0.05CN, and PVA-0.025CNT-0.025CN)

No.	Composite	Number of figures	Roughness average (nm)	Root mean square of roughness (nm)
1	Blank PVA	14-a	0.547	0.901
2	PVA+0.05 CNT	14-b	0.979	1.52
3	PVA+0.05 CN	14-c	1.17	1.79
4	PVA+0.025CNT+0.025CN	14-d	4.86	6.18

REFERENCES

[1] Abdullah, Z. W.; Dong, Y.; Davies, I. J.; Barbhuiya, S., PVA, PVA Blends, and Their Nanocomposites for Biodegradable Packaging Application, *Polym. Plast. Technol. Eng.* **2017**, *56*, 1307-1344, https://doi.org/10.1080/03602559.2016.1275684.

[2] Saini, I.; Sharma, A.; Dhiman, R.; Aggarwal, S.; Ram, S.; Sharma, P. K., Grafted SiC nanocrystals: For enhanced optical, electrical and mechanical properties of polyvinyl alcohol, *J. Alloy. Compd.* **2017**, *714*, 172-180, https://doi.org/10.1016/j.jallcom.2017.04.183.

[3] Marin, E.; Rojas, J.; Ciro, Y., A Review of polyvinyl alcohol derivatives: Promising materials for pharmaceutical and biomedical applications, *Afr. J. Pharm. Pharmacol.* **2014**, *8*, 674-684, DOI: 10.5897/AJPP2013.3906.

[4] Aslam, M.; Kalyar, M. A.; Raza, Z. A., Fabrication of reduced graphene oxide nanosheets doped PVA composite films for tailoring their opto-mechanical properties, *Appl. Phys. A123* **2017**, *424*, 1-12, https://doi.org/10.1007/s00339-017-1035-x.

[5] Sharma, S. K.; Prakash, J.; Pujari, P. K., Effect of molecular level dispersion of Graphene Oxide on free volume characteristics of Poly(vinyl alcohol) and its impact on thermal and mechanical properties of their nanocomposites, *Phys. Chem. Chem. Phys.* **2015**, *17*, 29201-29209, https://doi.org/10.1039/C5CP05278E.

[6] Gahlot, S.; Sharma, P. P.; Kulshrestha, V.; Jha, P. K., SGO/SPES-Based Highly Conducting Polymer Electrolyte Membranes for Fuel Cell Application, *ACS Appl. Mater. Interfaces* **2014**, *8*, 5595-5601, DOI: 10.1021/am5000504.

[7] Aslam, M.; Kalyar, M. A.; Raza, Z. A., Graphene oxides nanosheets mediation of poly(vinyl alcohol) films in tuning their structural and opto-mechanical attributes, *J. Mater. Sci. Mater. Electron.* **2017**, *28*, 13401-13413, https://doi.org/10.1007/s10854-017-7177-y.

[8] Weidenfeller B.; Höfer M.; Schilling F. R., Thermal conductivity, thermal diffusivity, and specific heat capacity of particle filled polypropylene. *Compos Part A Appl. Sci. Manuf*., **2004**, *35*, 423-429, https://doi.org/10.1016/j.compositesa.2003.11.005.

[9] Gan, H.; Yuan, J.; Zhang, Y.; Li, S.; Yu, L.; Wang, J.; Hu J.; Yang, N.; Xue, Z., Electrospun Composite Gel Polymer Electrolytes with High Thermal Conductivity toward Wide Temperature Lithium Metal Batteries. *ACS Appl. Energy Mater.*, **2021**, *8*8, 130-8141, https://doi.org/10.1021/acsaem.1c01420.

[10] Sharma, S. K.; Sudarshan, K.; Pujari, P. K., Unraveling the sub-nanoscopic structure at interphase in a poly(vinyl alcohol)-MOF nanocomposite, and its role in thermo-mechanical properties. *Phys. Chem. Chem. Phys.*, **2016**, *18*, 25434-25442, https://doi.org/10.1039/C6CP04872B.

[11] Falkovich, S. G.; Nazarychev, V. M.; Larin, S. V.; Kenny, J. M.; Lyulin, S. V., Mechanical Properties of a Polymer at the Interface Structurally Ordered by Graphene. *J. Phys. Chem. C* **2016**, *12*, 6771-6777, https://doi.org/10.1021/acs.jpcc.5b11028.

[12] Utpalla, P.; Sharma, S. K.; Prakash, J.; Bahadur, J.; Sahu, M.; Pujari, P. K., Free volume structure at interphase region of poly (ethylene oxide)-Al_2O_3 nanorods composites based solid polymer electrolyte and its direct correlation with Li ion conductivity. *Solid State Ionics*, **2022**, *375*, 115840, https://doi.org/10.1016/j.ssi.2021.115840.

[13] Hussain, F.; Hojjati, M.; Okamoto M.; Gorga, R. E., Review article: Polymer-matrix Nanocomposites, Processing, Manufacturing, and Application: An Overview. *J. Comp. Mater.* **2006**, *40*, 1511-1575, https://doi.org/10.1177/002199830606.

[14] Hou, C. -H.; Liu, N. -L.; Hsu, H. -L., Walter Den, Development of Multi-Walled Carbon Nanotube/Poly(vinyl Alcohol) Composite as Electrode for Capacitive Deionization, Separation and Purification Technology, *Sep. Purif. Technol.* **2014**, *130*, 7-14, https://doi.org/10.1016/j.seppur.2014.04.004.

[15] Das, A. K.; Sinha, S.; Mukherjee, A.; Meikap, A. K., Enhanced dielectric properties in polyvinyl alcohol-Multiwall carbon nanotube composites. *Mater. Chem. Phys.* **2015**, *167*, 286-294, https://doi.org/10.1016/j.matchemphys.2015.10.045.

[16] Dilshad, M. R.; Islam, A.; Haider, B.; Sabir, A.; Ijaz, A.; Khan, R. U.; Durrani, A. K., Novel PVA/PEG nano-composite membranes tethered

with surface engineered multiwalled carbon nanotubes for carbon dioxide separation, *Microporous Mesoporous Mater.* **2020**, *308*, 110545, https://doi.org/10.1016/j.micromeso.2020.110545.

[17] Hassanien, A. S.; Hatem Alamri, R..; El Radaf, I. M., Impact of film thickness on optical properties and optoelectrical parameters of novel $CuGaGeSe_4$ thin films synthesized by electron beam deposition, *Opt. Quantum Electron.* **2020**, *52*, 335, 1-18, https://doi.org/10.1007/s11082-020-02448-9.

[18] Cisneros, J. I., Optical characterization of dielectric and semiconductor thin films by use of transmission data, *Appl. Opt.* **1998**, *37*, 5262-5270, https://doi.org/10.1364/AO.37.005262.

[19] Nwofe, P. A.; Reddy, K. T. R.; Tan, J. K.; Forbes, I.; Miles, R. W., Thickness dependent optical properties of thermally evaporated SnS thin films, *Phys. Procedia* **2012**, *25*, 150-157, https://doi.org/10.1016/j.phpro.2012.03.064.

[20] Allen, G. C.; Swallow, G. A., Reflectance spectroscopy of oxide films. II. Oxide layers on chromium metal, *Oxid. Met*. **1982**, *17*, 157-176, https://doi.org/10.1007/BF00606198.

[21] Mohamed, M. B.; Abdel-Kader, M. H., Effect of excess oxygen content within different nano-oxide additives on the structural and optical properties of PVA/PEG blend, *J. Appl. Phys*. *A* **2019**, *209*, https://doi.org/10.1007/s00339-019-2492-1.

[22] Al-Taa'y, W.; Nabi, M. A.; Yusop, R. M.; Yousif, E.; Abdullah, B. M.; Salimon, J.; Salih, N.; Zubairi, S. I. Effect of Nano ZnO on the Optical Properties of Poly(vinyl chloride) Films,*Int. J. Polym. Sci.* Vol. **2014**, Article ID 697809, 1-6, https://doi.org/10.1155/2014/697809

[23] Al-Taa'y, W. A.; Ameer, A. A.; Al-Dahhan, W. H.; Abddallh M.; Yousif, E., Optical constants of poly(vinyl chloride) doped by nano ZnO, *J. Chem. Pharm. Res.* **2015**, 7, 536-541.

[24] Hassen, A.; El Sayed, A. M.; Morsi, W. M.; El-Sayed, S., Preparation, Influence of Cr_2O_3 nanoparticles on the physical properties of polyvinyl alcohol, *J. Appl. Phys.* **2012**, *112*, 093525-1-8, https://doi.org/10.1063/1.4764864.

[25] Soliman, T. S.; Vshivkov, S. A., Effect of Fe nanoparticles on the structure and optical properties of polyvinyl alcohol nanocomposite films, *J. Non-Cryst. Solids* **2019**, *519*, 119452, https://doi.org/10.1007/s00289-020-03115-5.

[26] Augustine, M. S.; Jeeju, P. P.; Sreevalsa, V. G.; Jayalekshmi, S., Enhanced photoluminescence in transparent thin films of polyaniline-zinc oxide nanocomposite prepared from oleic acid modified zinc oxide nanoparticles, *Thin Solid Films* **2014**, *562*, 84-89, https://doi.org/10.1016/j.tsf.2014.03.083.

[27] Al-Bataineh, Q. M.; Alsaad, A. M.; Ahmad, A. A.; Al-Sawalmih, A., Structural, Electronic and Optical Characterization of ZnO Thin Film-Seeded Platforms for ZnO Nanostructures: Sol-Gel Method Versus *Ab Initio* Calculations. *J. Electron Mater*. **2019**, *48*, 5028-38, https://doi.org/10.1007/s11664-019-07303-6.

[28] Stamate, M. D., Dielectric properties of TiO_2 thin films deposited by a DC magnetron sputtering system, *Thin Solid Films* **2000**, *372*, 246-249, https://doi.org/10.1016/S0040-6090(00)01027-0.

[29] Souri, D.; Tahan, Z. E., A new method for the determination of optical band gap and the nature of optical transitions in semiconductors, *Int. J. Appl. Phys. B* **2015**, *119*, 273-279.

[30] Badawi, A., Engineering the optical properties of PVA/PVP polymeric blend in situ using tin sulfide for optoelectronics, *J. Appl. Phys. A* **2020**, *126*,335, https://doi.org/10.1007/s00339-020-03514-5.

[31] Mohamed, M. B.; Abdel-Kader, M. H., Effect of annealed ZnS nanoparticles on the structural and optical properties of PVA polymer nanocomposite, *Mater. Chem. Phys.* **2020**, *241*, 122285, https://doi.org/10.1016/j.matchemphys.2019.122285.

[32] Urbach, F. The long wavelength edge of photographic sensitivity and of the electronic absorption of solids, *Phys. Rev.* **1953**, *92*, 1324, https://doi.org/10.1103/PhysRev.92.1324.

[33] Heiba, Z. K.; Mohamed, M. B.; Imam, N. G., Structural tuning of CdS nanoparticles with nucleation temperature and its reflection on the optical properties, *J. Mol. Struct.* **2015**, *1094*, 91-97, https://doi.org/10.1016/j.molstruc.2015.04.003.

[34] Sharma, I.; Hassanien, A. S., Effect of Ge-addition on physical and optical properties of chalcogenide

$Pb_{10}Se_{90-x}Ge_x$ bulk glasses and thin films, *J. Non-Cryst. Solids* **2020**, *548*, 120326, https://doi.org/10.1016/j.jnoncrysol.2020.120326.

[35] Abdullah O. G.; Saber, D. R., Optical absorption of poly-vinyl alcohol films doped with nickel chloride, *Appl. Mech. Mater.* **2012**, 110-116, 177-182, https://doi.org/10.4028/www.scientific.net/AMM.110-116.177.

[36] Abed, R. N.; Abed, A. R. N.; Yousif, E., Carbon Surfaces Doped with (Co_3O_4-Cr_2O_3) Nanocomposite for High-Temperature Photo Thermal Solar Energy Conversion Via Spectrally Selective Surfaces, *Prog. Color Colorants Coat.* **2021**, *14*, 301-315, https://dx.doi.org/10.30509/pccc.2021.166749.1098.

[37] Hassanien, A. S.; Akl, A. A., Effect of Se addition on optical and electrical properties of chalcogenide CdSSe thin films, *Superlattice Microst.* **2016**, *89*, 153-169, https://doi.org/10.1016/j.spmi.2015.10.044.

[38] Hassanien, A. S., Intensive linear and nonlinear optical studies of thermally evaporated amorphous thin Cu-Ge-Se-Te films, *J. Non-Cryst. Solids* **2022**, *586*, 121563, https://doi.org/10.1016/j.jnoncrysol.2022.121563.

[39] Heiba, Z. K.; Mohamed, M. B.; Imam, N. G., Fine-tune optical absorption and light emitting behavior of the CdS/PVA hybridized film nanocomposite, *J. Mol. Struct.* **2017**, *1136*, 321-329, https://doi.org/10.1016/j.molstruc.2017.02.020.

[40] Abed, R. N.; Emad Abed, Y.; Rashad, A. R. N.; Alaa A., Synthesis Thin Films of Poly(Vinyl Chloride) Doped by Aromatic Organosilicon to Absorb the Incident Light, *Silicon* **2022**, https://doi.org/10.1007/s12633-022-01893-3.

[41] Al-Azzawi, Z. M.; Al-Baidhani, M.; Abed, A. R. N.; Abed, R. N., Influence of Nano Silicon Carbide (SiC) Embedded in Poly(Vinyl Alcohol) (PVA) Lattice on the Optical Properties, *Silicon* **2021**, https://doi.org/10.1007/s12633-021-01325-8.

[42] Sharma, I.; Sharma, P.; Hassanien, A. S., Optical properties and optoelectrical parameters of the quaternary chalcogenide amorphous $Ge_{15}Sn_xS_{35-x}Te_{50}$ films, *J. Non-Cryst. Solids* **2022**, *590*, 121673, https://doi.org/10.1016/j.jnoncrysol.2022.121673.

[43] Imam, N. G., Mohamed Bakr Mohamed, Environmentally friendly $Zn_{0.75}Cd_{0.25}S$/PVA heterosystem nanocomposite: UV-stimulated emission and absorption spectra, *J. Mol. Struct.* **2016**, *1105*, 80-86, https://doi.org/10.1016/j.molstruc.2015.10.039.

[44] Abed, A. N.; Abed, R. N., Characterization Effect of Copper Oxide and Cobalt Oxide Nanocomposite on Poly(Vinyl Chloride) Doping Process for Solar Energy Applications, *Prog. Color Colorants Coat.* **2022**, *15*, 235-241, https://dx.doi.org/10.30509/pccc.2021.166858.1123.

[45] Ghosh, B.; Olivos, F. G.; Gonzalez, R. E., Plasmon-enhanced optical absorption with graded bandgap in diamond-like carbon (DLC) films, *J. Mater. Sci.* **2017**, *52*, 218-228, https://doi.org/10.1007/s10853-016-0324-7.

[46] Hassanien, A. S.; Sharm, I., Dielectric properties, Optoelectrical parameters and electronic polarizability of thermally evaporated a-Pb-Se-Ge thin films, *Phys. B: Conden. Matter.* **2021**, *622*, 413330, https://doi.org/10.1016/j.physb.2021.413330.

[47] Abdolrahimi, M.; Seifi, M.; Ramezanzadeh, M. H., Study the effect of acetic acid on structural, optical and mechanical properties of PVA/chitosan/ MWCNT films, *Chin. J. Phys.* **2018**, *56*, 221-230, https://doi.org/10.1016/j.cjph.2017.12.018.

[48] Algethami, N.; Rajeh, A.; Ragab, H. M.; Tarabiah, A. E.; Gami, F., Characterization, optical, and electrical properties of chitosan/polyacrylamide blend doped silver nanoparticles, *J. Mater. Sci.: Mater. Electron*. **2022**, *33*, 10645-10656, https://doi.org/10.1007/s10854-022-08048-5.